ELSEVIER

Application of Direct Methods for Crystal Structure Determination Using Strongly Dynamical Bulk Electron Diffraction

W. Sinkler and L. D. Marks

Northwestern University, Department of Materials Science and Engineering, 2225 North Campus Drive, Evanston, IL 60208-3108

In recent work it was shown that dynamical diffraction effects on direct methods calculations can be taken into account, and that the effect of dynamical scattering is an approximate reconstruction of $|1 - \Psi(\mathbf{r})|$, where $\Psi(\mathbf{r})$ is the complex electron exit wave. The present work examines these approximations in more detail using the channeling theory and empirical examples. Despite a dependence on thickness and structure in the general case, the approximations are well justified for structures that consist of well-defined atomic columns along the beam direction. An overview of the present minimum relative entropy direct methods algorithm is presented.

INTRODUCTION

There are few methods that can provide direct real-space information concerning the bulk atomic structure of materials. Presently, techniques that do so fall into two broad groups: the first of these are high-resolution electron microscopy (HRTEM) and holographic techniques, which includes X-ray holography. These are, broadly speaking, techniques that use interference effects to directly obtain either an electron exit wave—using filters in the case of through-focus holography [1–3]—superposition of an undisturbed plane wave in the case of off-axis holography [4], and interference from an emitter atom in the case of X-ray photoelectron holography [5]. A second group that is well known to X-ray crystallographers, are so-called direct methods [6]. In contrast to the interference techniques, which utilize a physical effect to preserve the phase information in the recorded data, the diffraction data used by direct methods does not contain any phase information. Nevertheless, phase information may be restored based on probability arguments that rely on consistency of the data with expectations concerning the form of the real-space distribution. In the case of kinematical data from a high-quality single crystal, this forms a powerful basis for determining crystal structures. It has become routine in such cases to solve crystal structures with little human interference using computerized direct methods algorithms.

Obtaining a single crystal suitable for X-ray diffraction can be difficult, and in many cases impossible. In many practical situations one would like to know the structure of a small particle, perhaps embedded in an inhomogeneous sample. In such cases, X-ray techniques may be inapplicable, and for such instances it is necessary to optimize approaches using electron probes. Direct structure information may be obtainable using HRTEM, holography, or CBED. However, this information is often either constrained in its resolution, subject to large errors, or difficult to interpret. The application of direct methods with electron data to solve crystal structures has attracted increasing attention recently, particularly for solving organic crystalline

MATERIALS CHARACTERIZATION 42:283–295 (1999)

655 Avenue of the Americas, New York, NY 10010

1044-5803/99/$–see front matter
PII S1044-5803(99)00021-2

structures [7–9], or surface reconstructions [10–13]. More recently, the first steps have been made towards assessing the effects of dynamical distortions on direct methods calculations [14, 15]. It is the purpose of this work to continue this assessment and to consider new directions that would represent improvements in present strategies of using electron diffraction data within a direct methods context. Prior to considering the application of direct methods in a framework of dynamical diffraction, the following section will give some details and background on the present direct methods algorithm, and illustrate its application in a hypothetical case of kinematical electron diffraction. Following this, the dynamical case will be presented. To assess the effect of dynamical distortions on direct methods, it is necessary to generalize the nature of these distortions. This is difficult to do, because the dynamical diffraction effects perturb diffraction intensities in rather unpredictable ways. It has, nevertheless, recently been shown empirically [15] that the dynamical amplitudes $|\Psi(\mathbf{h})|$ for thicknesses up to approximately 200Å tend to scale with the Fourier components of the function $|1-\Psi(\mathbf{r})|$, where $\Psi(\mathbf{r})$ is the electron exit wave. Due to this scaling, as well as the presence of well-defined peaks in the function $|1-\Psi(\mathbf{r})|$ at the positions of projected atomic columns, direct methods tend to restore a function resembling $|1-\Psi(\mathbf{r})|$ in the dynamical case. It is the main purpose of the present work to examine this scaling in more detail using the electron channeling approximation to incorporate dynamical effects. As will be shown, the scaling is not general, but is dependent on both specimen thickness and on details of the crystal structure. The scaling is, nevertheless, a reasonable approximation, and a significant improvement on the kinematical approximation, to which it simplifies for small thicknesses. Because of the emphasis of light atoms in the function $|1-\Psi(\mathbf{r})|$, which typically occurs for specimen thicknesses in the range of 50–200Å, dynamical effects can lead to a pronounced emphasis of light atom positions in a structure, which can be used to provide initial light atom positions for subsequent structure refinement.

DIRECT METHODS ALGORITHM AND APPLICATION TO KINEMATICAL MODEL CASE

The general procedure followed in the present application of direct methods is described in [16]. A schematic illustrating the procedure is shown as Fig. 1. Prior to the actual procedure, beams whose phases are to be held fixed are specified. These may be, for example, phases used to define a unit cell origin (suppressing redundant solutions that are related by a translation), and others that may be fixed using information from HRTEM imaging or other techniques. Following this, a normalization of the raw data (the set $\{|F(\mathbf{h})|\}$) to obtain windowed unitary structure factors ($\{|U(\mathbf{h})|\}$) is undertaken as described in [16]. The application of the window serves to optimize the ability of the direct methods algorithm to recognize, and thus favor, solutions containing atom-like features [15, 16]. The procedure in which actual assignment of phases occurs consists of two nested loops. The outer loop (loop 1 in Fig. 1) is a global minimization of the figure of merit (FOM, see below) as a function of the choice of an auxiliary set of starting phases assigned in step 3. There are typically 10–20 beams whose phases are assigned in step 3, and the choice of phases is varied using a genetic algorithm as described in [17].

The inner loop 2 is the phase extension. It consists a forward and backward Fourier transforms, and between them the application of the minimum relative entropy operator to the real-space distribution $u_n(\mathbf{r})$ in an update scheme to obtain $u_{n+1}(\mathbf{r})$:

$$u_{n+1}(\mathbf{r}) = u_n(\mathbf{r})\ln\{u_n(\mathbf{r})/\langle u_n\mathbf{r}\rangle\} \qquad (1)$$

in which $<u_n(\mathbf{r})>$ is the mean value of $u_n(\mathbf{r})$. The forward transform involves those $U(\mathbf{h})$, which have phases assigned. Application of the update formula (1), and reverse FT results in a new set $\{U_{n+1}(\mathbf{h})\}$ which will

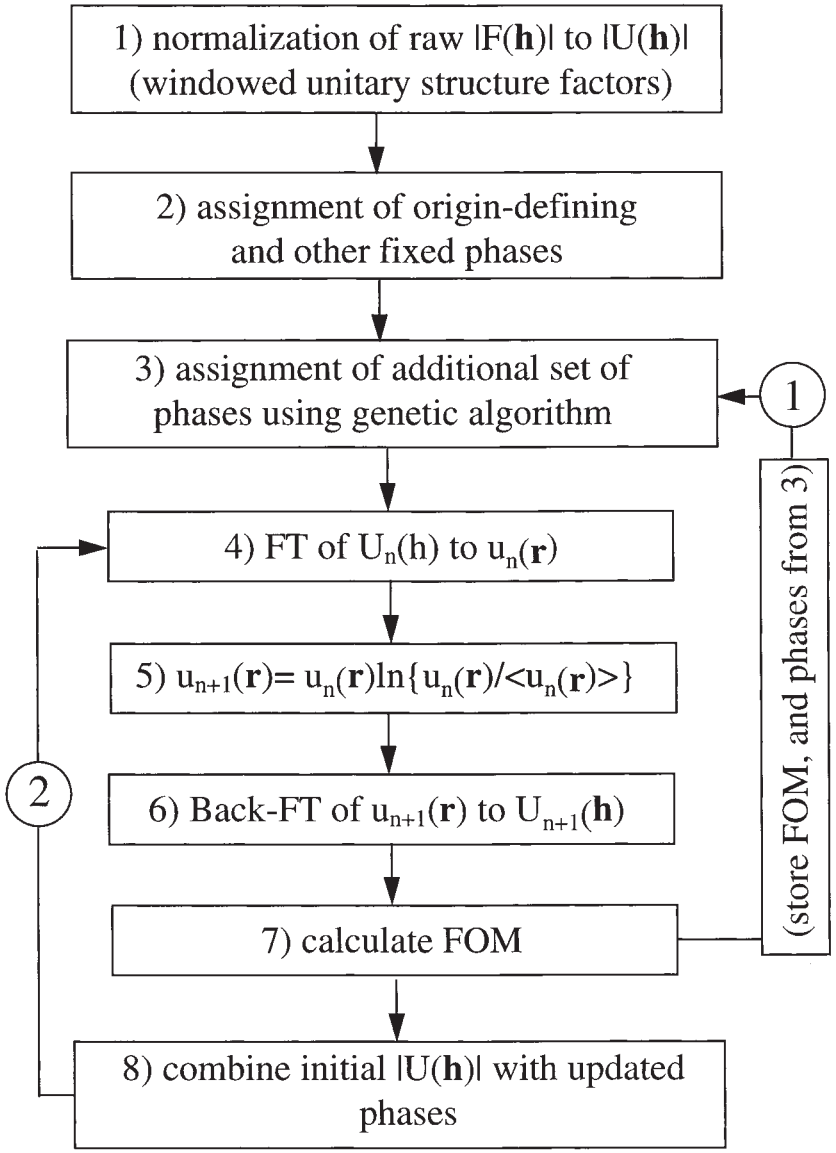

FIG. 1. Schematic of present direct methods algorithm. Loop 1 is controlled by the genetic algorithm, which optimizes phases set in 3) with respect to the FOM. Inner loop 2 is the phase extension.

differ from the $\{U_n(\mathbf{h})\}$ in both amplitudes and phases. The degree to which they differ is a measure of the self-consistency of the initial set, and is used to calculate the self-consistency FOM given by:

$$FOM = \sum_h{}' |U_n(\mathbf{h}) - \beta U_{n+1}(\mathbf{h})| / \sum_h{}' |U_n(\mathbf{h})| \quad (2)$$

In Eq. (2), β is a constant that is chosen to minimize the FOM, and the prime on the sum excludes the $\mathbf{h} = 0$ beam. The FOM tests for the consistency of the prior $\{U_n(\mathbf{h})\}$ with the updated $\{U_{n+1}(\mathbf{h})\}$, which have been altered by the application of Eq. (1). Thus, the FOM will be small if the effect of the update is roughly a scaling (by β) of the $U_n(\mathbf{h})$, and it will be large if the initial $U_n(\mathbf{h})$ are dramatically altered, and are thus inconsistent with the minimum relative entropy operator.

Because of the nonlinearities in Eq. (1), the set $\{U_{n+1}(\mathbf{h})\}$ contains predictions of the

phase and amplitude of beams that were not present in the initial set $\{U_n(\mathbf{h})\}$. In initiating the subsequent cycle of loop 2, strongly indicated update phases (for all except the beams specified in step 2) are coupled with the initial amplitudes $|U(\mathbf{h})|$ to begin the next cycle of the phase extension. Loop 2 is cycled repeatedly as long as the FOM decreases, at which point it is halted, the FOM is recorded as a characteristic of the set of phases specified by the genetic algorithm in step 3, and a new set is assigned. The phases controlled by the genetic algorithm are thus optimized using the FOM by repetition of loop 1. The top solutions or individuals are stored for inspection.

The most crucial part of the process is the minimum relative entropy operator, as it is from this that the phase updates are obtained. As is shown in [15, 16], iterative application of Eq. (1) tends to minimize the relative entropy, which is consistent with (absolute) entropy maximization. It thus yields a final $u(\mathbf{r})$ that is both consistent with the data as well as most probable in an information theory sense. An alternative view of Eq. (1) is as a sharpening operator, which tends to emphasize and sharpen the peaks that are already present in the initial distribution $u_n(\mathbf{r})$, and conversely, to create a low, smooth background in those $\mathbf{r}$ regions for which $u_n(\mathbf{r})$ is small. The effect of the minimum entropy operator on the projected atomic potential of a molybdenum atom is shown in Fig. 2, from which the sharpening effect is evident. For kinematical diffraction data, the real space distribution (i.e., the $u(\mathbf{r})$ when all phases in the Fourier representation are correct) is simply the potential distribution. The latter is characterized by sharp peaks at the atom sites, and relatively flat interatomic regions. Therefore, the sharpening of initial peaks, plus the suppression of background, creates from $U_n(\mathbf{r})$ a more probable $U_{n+1}(\mathbf{r})$.

Figure 4(a) shows a model potential based on the $(Ga,In)_2SnO_5$ structure, which was recently solved using direct methods and dynamical diffraction [14, 15]. A ball-and-stick model of the structure is shown

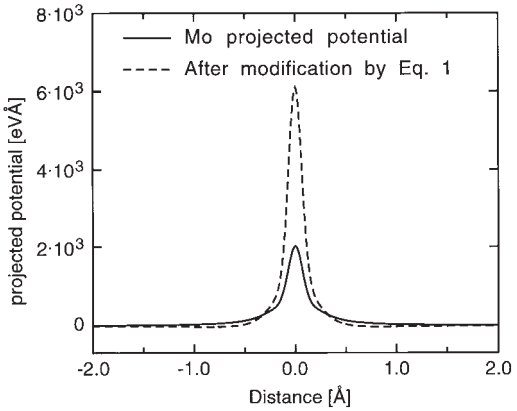

FIG. 2. Illustration of the effect of the minimum relative entropy sharpening operator [Eq. (1)] on the projected atomic potential of molybdenum [25]. In calculating the average, a radius of 1.25Å was assumed, based on the column density in the [100] projection of bcc Mo.

for comparison in Fig. 3. The calculated kinematical diffraction data set for this structure in [001] projection were input into the direct methods algorithm, using only two origin-defining phases in step 2. The top solutions in this case all had strong peaks in roughly the positions shown in Fig. 4(b). As can be seen, although the solution does not correctly identify the structure, the peaks bear a strong resemblance to the cation structure, but with a shift of $\approx$[0,0,1/6]. By fixing the phases of two additional strong beams, correct registry of the cation structure is obtained, and some of the oxygen atoms are correctly indicated, as shown in Fig. 4(c). It is often possible to obtain structure factor phase information from HRTEM images. Although the strong interaction introduces some uncertainty in the phases due to dynamical effects, the phase information from a conventional HRTEM image tends to be reliable for the thinnest available regions, for strong diffracted beams, and for beams of small spatial frequency [15]. By fixing the phases of 18 beams in the data set to 0° or 180° based on an experimental HRTEM image [14], the reconstruction shown in Fig. 4(d) is obtained. Despite the fact that not all fixed phases are correct, Fig. 4(d) is nearly indistinguishable form the calculated potential in Fig. 4(a),

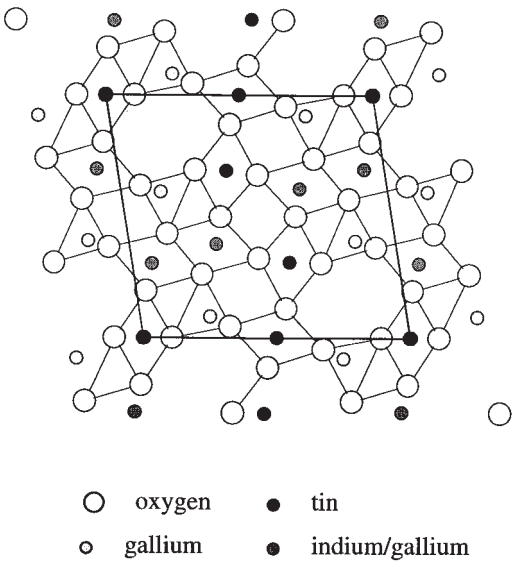

FIG. 3. Ball-and-stick model of $(Ga,In)_2SnO_5$, viewed along [010]. Length of the horizontal axis (a-axis) is 11.69Å.

and clearly indicates the positions of all atoms in the structure.

As is evident from Fig. 4, direct methods does not unambiguously solve the phase problem in a general sense. It, nevertheless, dramatically reduces the number of unknowns to a small and manageable set. By setting four properly chosen phases (one of four possible choices for the nonorigin-defining beams), the cation distribution is revealed. With 18 phases set from an experimental HRTEM image, the entire structure is revealed in this model kinematical case. Without direct methods, the phase problem for the present centrosymmetric case would have on the order of 2^{100} solutions, with no way to distinguish among them.

APPLICATION TO STRONGLY DYNAMICAL DIFFRACTION DATA

As shown in the above section, by using direct methods with high-quality kinematical diffraction the phase problem becomes tractable. In the case of electron diffraction, however, it is only in rare cases that one can consider dynamical effects as a minor perturbation of the measured intensities. This can, for instance, be assumed with some validity for the case of a single atomic layer, and electron diffraction may thus be assumed to be largely kinematical in the case of diffraction from the atoms in a surface reconstruction. A number of surface structures have been solved recently by applying direct methods to plan view electron diffraction data sets [10–13]. Nevertheless, it is straightforward to show using multislice calculations that there is typically significant deviation from kinematical conditions at about 10Å thickness for inorganic materials with elements as heavy as Fe. While the situation is somewhat better for organic structures containing only elements with $Z \leq 8$, the diffraction data is, nevertheless, strongly affected by dynamical effects at thicknesses of 50Å, which are typical for a thin transmission electron microscope sample. In utilizing direct methods with dynamical diffraction, it is, therefore, necessary to consider how this affects the measured intensities, and how, in turn, the dynamically perturbed intensities alter the course of the direct methods calculations.

In previous work, it was shown that application of direct methods to dynamical electron diffraction data tends to result in solutions that resemble the function $|1-\Psi(\mathbf{r})|$ for the structure and zone axis direction studied [15]. The two reasons for this are, first, a scaling of the dynamical diffracted amplitudes with the Fourier coefficients of the function $|1-\Psi(\mathbf{r})|$, and second, because of the presence of atom-like peaks in the function $|1-\Psi(\mathbf{r})|$, which makes $|1-\Psi(\mathbf{r})|$ a probable outcome of a direct-methods calculation. The tendency of the diffraction amplitudes [which are the square root of the intensities $I(\mathbf{h})$] to scale with the Fourier coefficients of $|1-\Psi(\mathbf{r})|$ is illustrated in Fig. 5(a) for the $(Ga,In)_2SnO_5$ structure, at a thickness of 100Å [15].

The scaling illustrated in Fig. 5(a) can be understood based on the electron channeling theory [18–22]. The channeling theory makes a continuum approximation to the specimen potential along the beam direction, which is equivalent to making a zero-

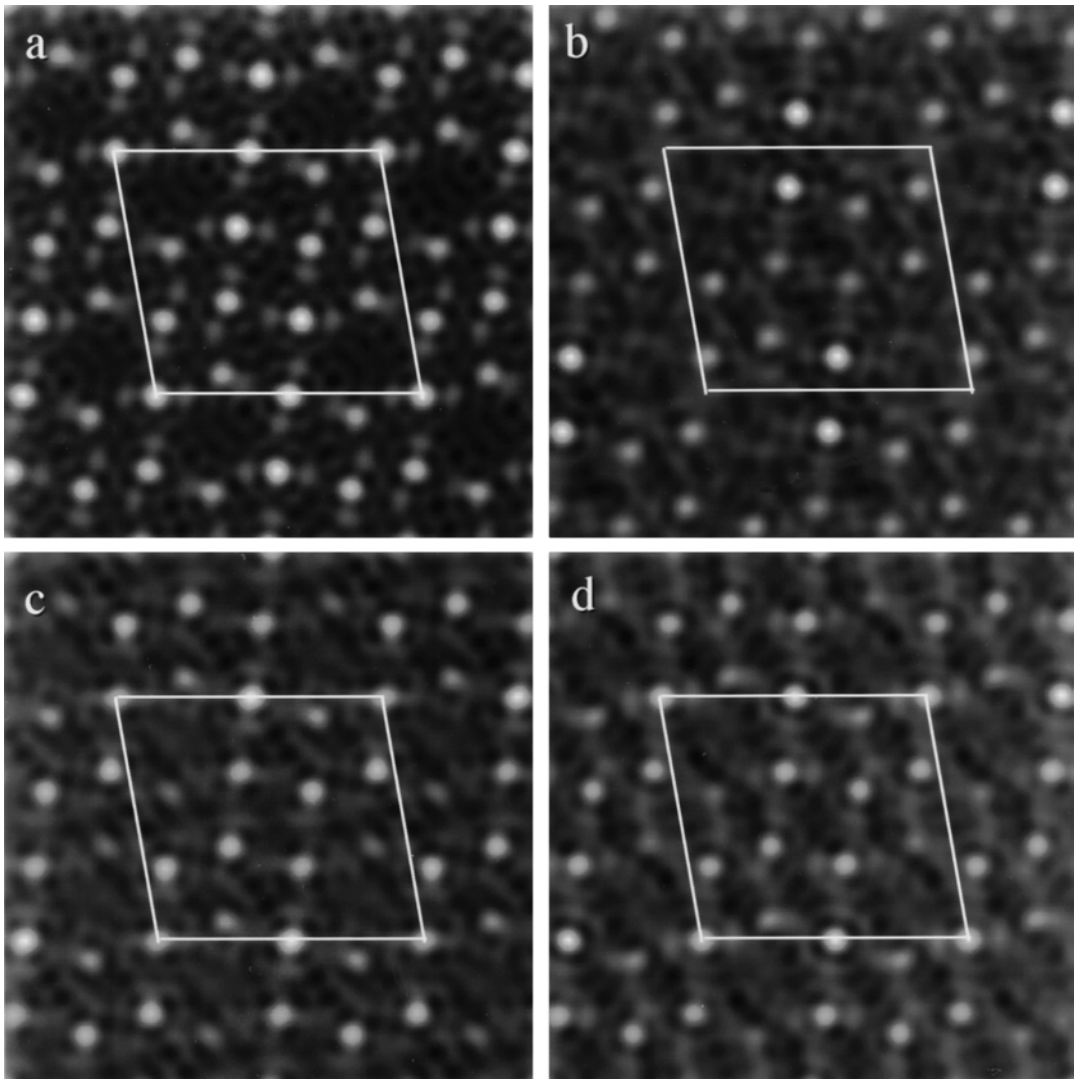

FIG. 4. a) Calculated projected potential of $(Ga,In)_2SnO_5$ along [010]. Length of the horizontal axis is 11.69Å. (b) Direct methods solutions using the Fourier components of (a) with two fixed phases for origin definition. (c) As (b), but with four fixed phases. (d) As (a), (b) but with 18 phases fixed based on experimental HRTEM image phases.

order Laue zone (ZOLZ) approximation, and in addition, the excitation errors are ignored. Nevertheless, a qualitative validity is maintained for on-zone diffraction, while a significant reduction in complexity of the three-dimensional wave equation for high energy electrons is achieved. The three-dimensional theory [23] is reduced to a wave equation in two dimensions, perpendicular to the beam direction. The result is an expression of the total wave as a superposition of the two-dimensional wavefunctions $\varphi_n(\mathbf{R})$ [where $\mathbf{R} = (x,y)$], each with a characteristic oscillation along the beam direction (the z direction):

$$\psi(\mathbf{R},z) = \sum_n C_n \Phi_n(\mathbf{R}) \exp\left\{-i\pi \frac{E_n}{E_0} kz\right\} \qquad (3)$$

The frequency of the oscillation is determined by the eigenvalue E_n associated with state Φ_n. In Eq. (3), E_0 is the incident beam energy, $k = \sqrt{(2mE_0)}/h$ and C_n is the excitation of the normalized eigenstate Φ_n. Much

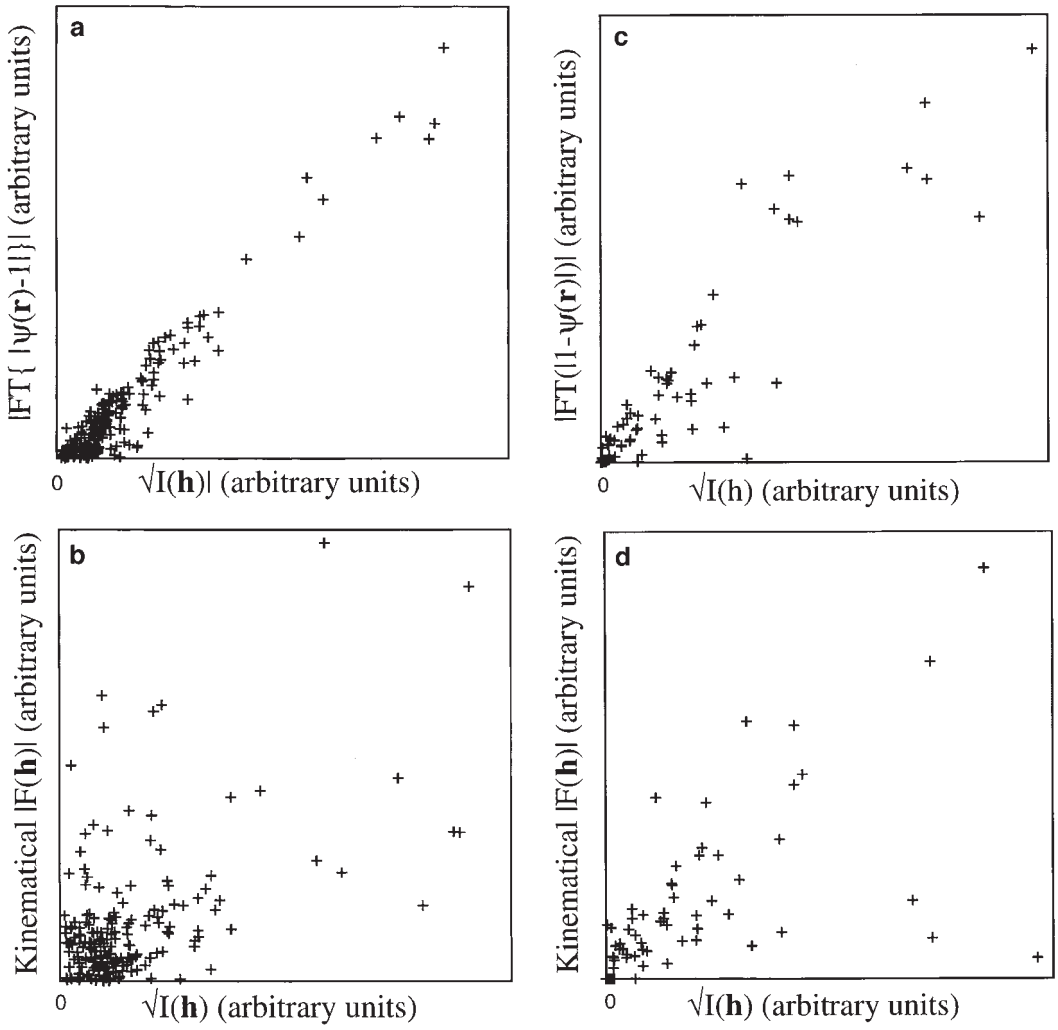

FIG. 5. (a) Plot of the moduli of Fourier components of $|1-\Psi(\mathbf{r})|$ versus $\sqrt{I}(\mathbf{h})$ for the $(Ga,In)_2SnO_5$ structure at 100Å thickness [15]. (b) Plot of kinematical structure factor moduli $|F(\mathbf{h})|$ versus $\sqrt{I}(\mathbf{h})$ for $(Ga,In)_2SnO_5$ at 100Å thickness [15]. (c) As (a), but for the Ca-doped $YSr_2Cu_2GaO_7$ structure at 113Å. (d) As (b), but with $\sqrt{I}(\mathbf{h})$ for $YSr_2Cu_2GaO_7$ structure at 113Å.

of the power of the channeling approximation lies in the fact that there are typically only a small number of bound states with significant excitation contributing to the wave. In addition to bound states, there is a continuum of unbound states in Eq. (3), which must exist to satisfy the boundary condition at the entrance face of the foil, which, for the unit plane wave incidence is

$$\sum_n C_n \Phi_n = 1.$$

For structures consisting of well-separated atomic columns along the beam direction, the symmetry of the projected potential reduces the eigenfunctions to those with *s*-like radial symmetry, of which there are at most three that contribute for even the heaviest atoms at typical accelerating voltages of 200–400keV and atomic separations of ≈3Å. For atoms lighter than Fe, the wave tends to be dominated by the 1s bound state, whose form is particularly simple, being approximately proportional to the projected atomic potential [15]. When both the 1s state is predominant, and the potential overlap of adjacent atomic columns is small, one can approximate the electron

exit wave as suggested by Van Dyck and Op de Beeck [22]:

$$\psi(\mathbf{R},z) = 1 - \sum_i C_i \Phi_i(\mathbf{R}-\mathbf{R}_i) \left(1 - \exp\left(-i\pi \frac{E_i}{E_0} kz\right)\right) \quad (4)$$

where the sum is over all N atoms in the unit cell, and Φ_i is the 1s channeling eigenstate for the atomic column centered at position $\mathbf{R}_i$. This considers the exit wave as made up of the separate contributions of atomic columns at $\mathbf{R}_i$, and approximates the total unbound states in the interstitial regions as ≈ 1.

From Fig. 5(a), the diffraction intensities $I(\mathbf{h}) = \Psi(\mathbf{h})\Psi^*(\mathbf{h})$ should scale with $FT(|1-\Psi(\mathbf{r})|)^2$. Taking the Fourier transform of Eq. (4) one obtains:

$$\Psi(\mathbf{h}) = \delta(0) - \sum_i C_i \Phi_i(\mathbf{h}) \exp(2\pi i \mathbf{h}\mathbf{R}_i) (1 - \exp(-2\pi i K_i z) \quad (5)$$

in which

$$K_i = \frac{E_i}{2E_0} k.$$

Taking the absolute square of Eq. (5), and ignoring terms with $\delta(0)$ results in:

$$I(\mathbf{h}) = \sum_i C_i^2 \Phi_i^2 \cdot 4\sin^2 \pi K_i z + \sum_{i<j} C_i C_j \Phi_i \Phi_j 8 \sin \pi K_i z \cdot \sin \pi K_j z \cdot \cos[2\pi \mathbf{h}(\mathbf{R}_i - \mathbf{R}_j) + \pi z(K_i - K_j)] \quad (6)$$

From Eq. (4) the function $|1-\Psi(\mathbf{r})|$ is:

$$|1 - \psi(\mathbf{r})| = \sum_i C_i \Phi_i(\mathbf{R}) \sqrt{2 - 2\cos 2\pi K_i z} \quad (7)$$

The square of the Fourier transform of Eq. (7) is:

$$FT\{|1-\psi(\mathbf{r})|\}^2 = \sum_i C_i^2 \Phi_i^2 \cdot 4\sin^2 K_i z + \sum_{i<j} C_i C_j \Phi_i \Phi_j \cdot 8 |\sin \pi K_i z| |\sin \pi K_j z| \cdot \cos 2\pi \mathbf{h}(\mathbf{R}_i - \mathbf{R}_j) \quad (8)$$

where use has been made of the equality

$$\sqrt{2 - 2\cos 2\pi K_i z} = |2 \sin \pi K_i z|.$$

There are clear similarities between Eqs. (6) and (8). The first term of both equations is identical, and the only differences are in the presence of the absolute value sine functions in Eq. (8), and in the additional interference terms in the argument of the cosine in Eq. (6). Concerning the absolute values in Eq. (8), these do not matter unless $z > 1/K_i$, which is the first crossing through zero of the sine function. For an isolated atomic column of tin atoms, the heaviest species in $(Ga,In)_2SnO_5$, the 1s eigenvalue is ≈ -200eV (for $E_0 = 300$kV, and B = 0.3Å^2), and the first crossover occurs at nearly 60Å. For thickness beyond this, the absolute values in Eq. (8) may cause discrepancies between Eqs. (6) and (8). However, these discrepancies only arise in terms involving tin and some other atom, and only when neither of the sine terms is small.

The additional term in the argument of the cosine in Eq. (6) can cause a real difference between Eqs. (6) and (8) whenever the thickness suffices to make it significant. Nevertheless, some cancellation of its effect can be expected, resulting in approximate agreement between Eqs. (6) and (8). In particular, the sine terms in Eq. (6) will be largest when $K_i z \approx (2n+1)/2$ and $K_j z \approx (2m+1)/2$. Assuming these values for $K_i z$ and $K_j z$, the cosine term in Eq. (6) reduces to $\pm \cos 2\pi h(R^i - R^j)$, where the sign is positive for m,n both even or both odd, and negative otherwise. From this, the sign on the cosine term will cancel the sign on the sine terms in Eq. (6) to produce agreement with Eq. (8) for the assumed values of $K_i z$ and $K_j z$. Some systematic simplification of the largest terms in the second sum of Eq. (6) can, therefore, be expected, causing them to agree with Eq. (8).

As can be seen in Fig. 5(a), these assumptions and approximations are justified for the $(Ga,In)_3SnO_5$ structure at a thickness of 100Å. By contrast, a kinematical approximation gives a considerably worse correlation, as shown in Fig. 5(b). Nevertheless,

the correlation between $\sqrt{I(\mathbf{h})}$ and $|FT(|1-\Psi(\mathbf{r})|)|$ is not perfect, and it is thickness and structure dependent. This is illustrated by considering another structure, that of a Ca-doped $YSr_2Cu_2GaO_7$ superconductor [24], in [001] projection. The correlation between $\sqrt{I(\mathbf{h})}$ and $|FT(|1-\Psi(\mathbf{r})|)|$, shown for this structure at a thickness of 113Å (84 slices) in Fig. 5(c), is noticeably weaker, either because of the structure dependence suggested by comparison of Eqs. (6) and (8), or because of restricted validity of the channeling approximation on which both Eqs. (6) and (8) rely. Despite the occasionally rather rough correlation found empirically, the likelihood that direct methods solutions will resemble $|1-\Psi(\mathbf{r})|$ is the best approximation presently available. It is a definite improvement on the kinematical approximation, to which it reduces as z approaches zero.

SENSITIVITY TO LIGHT ELEMENTS

A sensitivity to light elements has been demonstrated in direct methods using strongly dynamical electron diffraction intensities, both in experimental cases [14, 15], as well as using simulated data sets [15]. Figure 6(a) shows a direct methods result obtained using modeled intensities from multislice calculations for the $(Ga,In)_2SnO_5$ structure at a thickness of 113Å (36 repeat distances along the b-axis). In the direct methods calculation, 18 phases were fixed to the same values used in the obtaining Fig. 4(d), that is, those obtained from an experimental HRTEM image of the structure [14, 15]. Overlaid on the solution is a ball-and-stick model showing the oxygen atom positions of the structure. By comparing Figs. 6(a) and 4(d) it is clear that the effect of dynamical distortions to the intensities has been a shift in sensitivity toward the light oxygen atoms. Direct methods results using strongly dynamical electron diffraction data thus differ distinctly from those expected based on the kinematical approximation. Similar results have been obtained experimentally, and Fig. 6(a) bears a strong resemblance to a direct methods result obtained using experimental electron diffraction, which was used to solve the $(Ga,In)_2SnO_5$ structure [14]. The corresponding calculated $|1-\Psi(\mathbf{r})|$ is shown in Fig. 6(b), and, as can be seen, it is characterized by strong peaks at the oxygen positions in the structure. This indicates that the present case can be understood based on the correlation between $|1-\Psi(\mathbf{r})|$ and the direct methods solutions obtained from $I(\mathbf{h})$, which was the subject of the previous section. Because dynamical effects at thicknesses on the order of 50–200Å tend to emphasize light elements in $|1-\Psi(\mathbf{r})|$, direct methods using dynamical electron diffraction can be a useful technique for detecting the positions of light elements such as oxygen in bulk crystal structures.

Figures 7(b) and (c) show similar results for the Ca-doped $YSr_2Cu_2GaO_7$ structure, again using modeled data for 113Å (84 slices). In addition to the model diffraction data, 11 phases were fixed to values obtained from an experimental HRTEM image. In contrast to the $(Ga,In)_2SnO_5$ structure, the gallate superconductor does not resolve particularly well into distinctly separated atomic columns parallel to the beam direction. This is particularly true in the blocking layer centered on gallium, in which oxygens and cations partially overlap. The direct methods solution, [Fig. 7(a)], does not reveal the oxygen in the active layer, and is in reasonable agreement with the calculated $|1-\Psi(\mathbf{r})|$ in this region. However, in the blocking layer the structure is poorly revealed. In addition to overlap of atoms, the direct methods solution and $|1-\Psi(\mathbf{r})|$ may differ due to the relatively poor scaling of $\sqrt{I(\mathbf{h})}$ with $|FT(|1-\Psi(\mathbf{r})|)|$ for this structure, illustrated above in Fig. 5(c). A test of which effect (atomic overlap or poor scaling) is responsible for the difference between Fig. 7(b) and (c) may be obtained by performing a direct methods calculation using the Fourier components of $|1-\Psi(\mathbf{r})|$ as input, as these will be subject to the effects of atomic overlap, but the scaling will be perfect. The result of

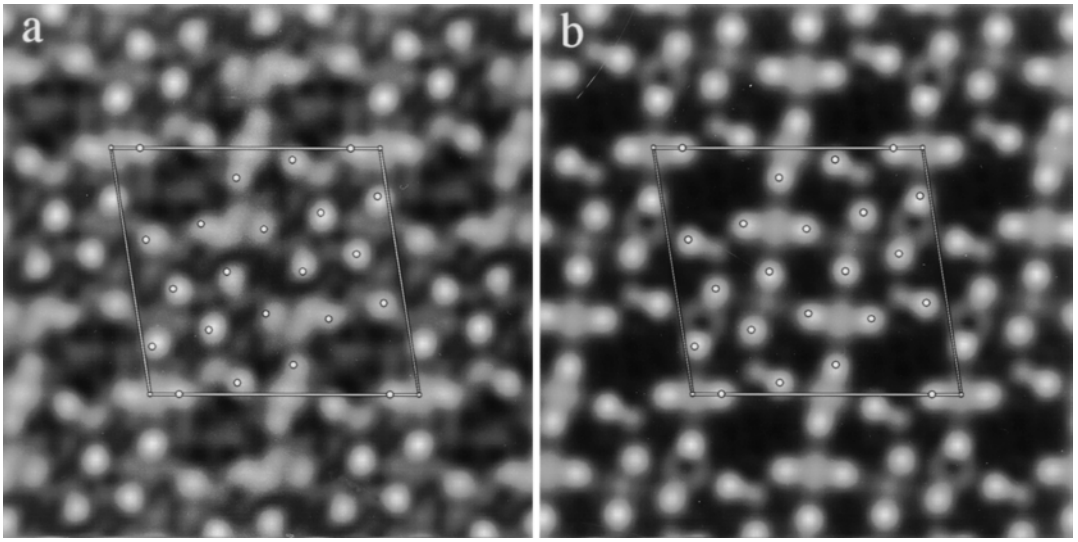

FIG. 6. (a) Direct methods solution using calculated intensities for $(Ga,In)_2SnO_5$ at 100Å thickness. Length of the horizontal axis is 11.69Å. (b) The function $|1-\Psi(\mathbf{r})|$ calculated with multislice for $(Ga,In)_2SnO_5$ at 100Å thickness.

this test is shown in Fig. 7(d). Although Fig. 7(d) does show peaks in the blocking layers that correspond roughly to the atomic column positions, it also contains peaks disagreeing with atomic columns, and does a slightly less good job of revealing the details of the active layers. Based on this, it is unclear whether the different performance of the present direct methods in the cases of the $(Ga,In)_2SnO_5$ and $YSr_2Cu_2GaO_7$ structures is due to the poor definition of the atomic columns, or to the weaker correlation of $\sqrt{I}(\mathbf{h})$ with $|FT(|1-\Psi(\mathbf{r})|)|$ illustrated in Fig. 5(c).

DISCUSSION

The present work has presented an overview of the minimum relative entropy direct methods algorithm, and illustrated how this algorithm can be effective in reducing the number of unknowns in the phase problem. This approach is relatively new to the field of electron microscopy, and has large potential, both alone and in combination with other structure investigation techniques by complementing or filling in gaps in information obtained by other means. It has been presented in the present work in combination with image phases that were obtained from HRTEM, and some of the basic problems involving the treatment of dynamical effects have been investigated.

One particular strength of direct methods in combination with dynamical electron diffraction data is its potential for obtaining light atom positions in oxide structures. The reasons for this have been reviewed above, and the scaling between $\sqrt{I}(\mathbf{h})$ and the Fourier components of $|1-\Psi(\mathbf{r})|$ has been critically examined using the channeling theory, as well as empirically with multislice simulations. The channeling theory explains why this approximate scaling holds quite well for structures that resolve into well-defined atomic columns along the beam direction. Although the scaling property is thickness and structure-dependent in the general case, it nevertheless represents the best approximation available to account for the effects of dynamical distortions of intensities on the direct-methods solutions. It approximately accounts for dynamical effects, in some cases quite well for thicknesses on the order of 100Å or more [15]. As thickness goes toward zero, it converges to the kinematical approximation. However, for any structure of finite thick-

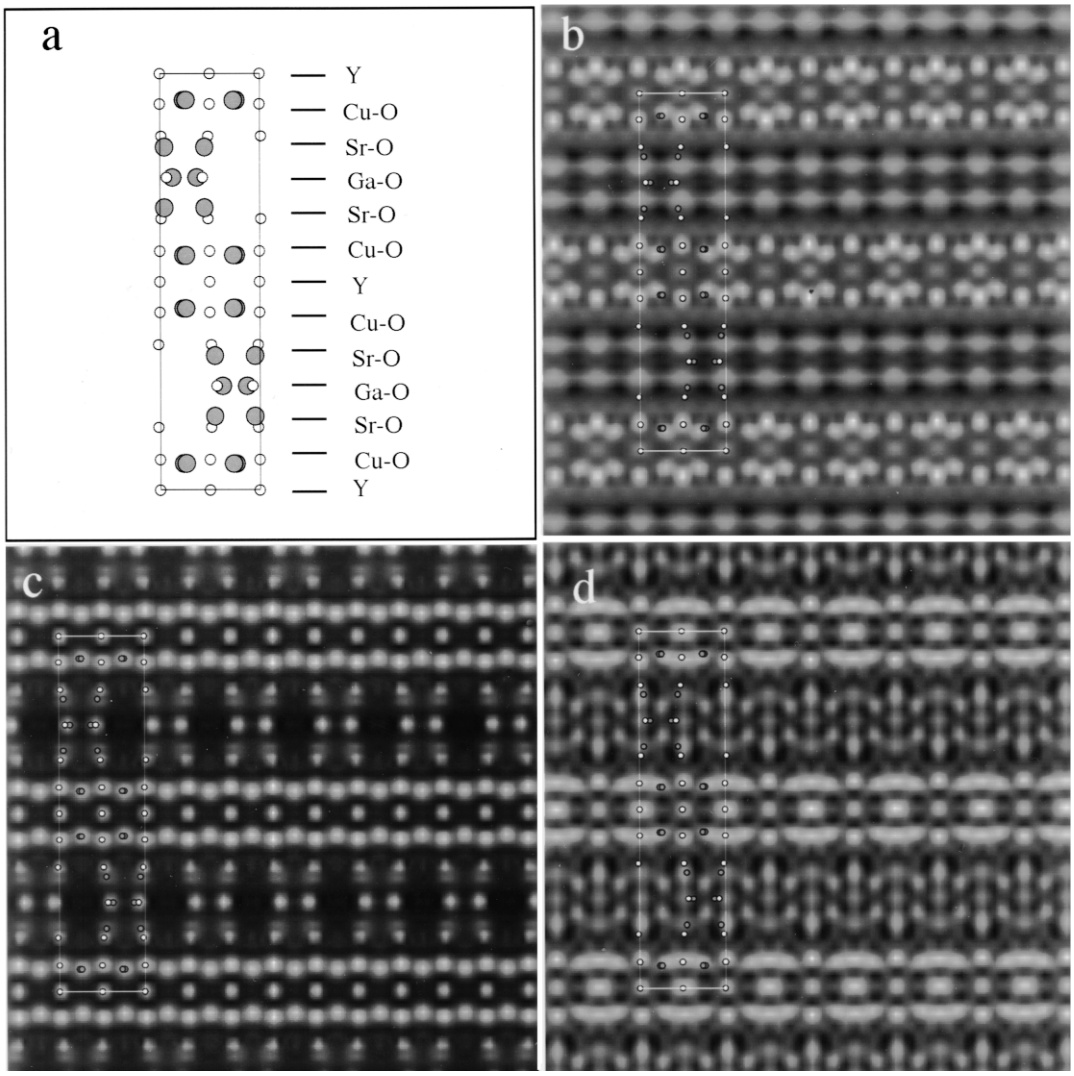

FIG. 7. (a) Ball-and-stick model of $YSr_2Cu_2GaO_7$, viewed along [001]. Oxygens are gray, cations are white. Scale is given by the vertical axis (a-axis) length of 22.8Å. (b) direct methods solution using calculated intensities for $YSr_2Cu_2GaO_7$ at 113Å thickness ([001] zone axis). (c) The function $|1-\Psi(\mathbf{r})|$ for Ca-doped $YSr_2Cu_2GaO_7$ structure at 113Å. (d) Direct methods solution using as input the Fourier components of (c).

ness it will be an improvement on the kinematical approximation, and it, thus, extends the regime of interpretability of direct methods into the attainable thickness range of real bulk samples. The strong correlation between the direct methods solution for $(Ga,In)_2SnO_5$ [Fig. 6(a)] and the calculated $|1-\Psi(\mathbf{r})|$ [Fig. 6(b)] is a direct consequence of the validity of the approximation for the case of $(Ga,In)_2SnO_5$.

Despite the viability of an approximate approach, it will never be possible a priori to be sure that a correlation between $\sqrt{I(\mathbf{h})}$ and the Fourier components of $|1-\Psi(\mathbf{r})|$ will exist in a given case, at least when no certain limit on the thickness can be specified. Because of this, and despite its usefulness as a technique for solving structures, an interpretational problem will always exist in the application of direct methods to dynamical diffraction data. The source of this uncertainty is effectively in the fact that the dynamical diffraction amplitudes are the Fourier components of an exit wave

that is complex, whereas the direct-methods solutions are constrained to be real by setting $U(-\mathbf{h}) = U^*(\mathbf{h})$. This suggests some interesting possibilities in removing this constraint, and allowing the direct-methods solutions to be complex. One would then no longer be constrained to an uncertain approximation in interpreting the results. However, it has yet to be shown that direct methods in the complex case can successfully restore an exit wave. Provided the ability to do this, there is a strong prospect for incorporating a direct methods approach into a yet broader variety of electron microscopic techniques, by employing direct-methods constraints and quantitative electron diffraction data to solve structural problems.

The authors would like to acknowledge helpful discussions with E. Landree. Support for this work from the National Science Foundation (DMR 91-20000) through the Science and Technology Center for Superconductivity is gratefully acknowledged.

References

1. P. Schiske: Image processing using additional statistical information about the object. In *Image Processing and Computer-Aided Design in Electron Optics*, P. W. Hawkes, ed., Academic Press, New York, p. 82 (1973).
2. W. O. Saxton: *Computer Techniques for Image Processing in Electron Microscopy*. Academic Press, New York (1978).
3. M. Op de Beeck, D. Van Dyck, and W. Coene: Focal series wave function reconstruction in HR-TEM. In *Electron Holography*, A. Tonomura, L. F. Allard, G. Pozzi, D. Joy, and Y. A. Ono, eds., Elsevier, Amsterdam, p. 307 (1995).
4. M. Lehmann and H. Lichte: Holographic reconstruction methods. In *Electron Holography*, A. Tonomura, L. F. Allard, G. Pozzi, D. Joy, and Y. A. Ono, eds., Elsevier, Amsterdam. p. 69 (1995).
5. M. Tegze and G. Faigel: X-ray holography with atomic resolution. *Nature* 380:49 (1996).
6. M. Woolfson and H.-F. Fan: *Physical and Non-Physical Methods of Solving Crystal Structures*, Cambridge University Press, Cambridge (1995).
7. D. L. Dorset: Is electron crystallography possible? The direct determination of organic crystal structures. *Ultramicroscopy* 38:23 (1991).
8. D. L. Dorset: *Structural Electron Crystallography*, Plenum Press, New York (1995).
9. C. J. Gilmore, C. J. Nicholson, and D. L. Dorset: Direct methods in electron crystallography—the *ab-initio* structure determination of 2 membrane protein structures in projection using maximum entropy and likelihood. *Acta Crystallogr.* 52:937 (1996).
10. L. D. Marks, R. Plass, and D. L. Dorset: Imaging surface structures by direct phasing. *Surf. Rev. Lett.* 4:1 (1997).
11. E. Landree, L. D. Marks, P. Zschack, and C. Gilmore: Structure of the TiO_2(100)-1×3 surface by Direct Methods. *Surface Sci.* 408:300–309 (1999).
12. C. Collazo-Davila, L. D. Marks, K. Nishii, and Y. Tanishiro: Atomic structure of the In on Si(111)(4×1) surface. *Surf. Rev. Lett.* 4:65 (1997).
13. C. J. Gilmore, L. D. Marks, D. Grozea, C. Collazo-Davila, E. Landree, and R. D. Twesten: Direct solutions of the Si(111) 7×7 structure. *Surface Sci.* 381:77 (1997).
14. W. Sinkler, L. D. Marks, D. D. Edwards, T. O. Mason, K. R. Poeppelmeier, Z. Hu, and J. D. Jorgensen: Determination of oxygen atomic positions in a Ga-In-Sn-O ceramic using direct methods and electron diffraction. *J. Solid State Chem.* 136:145 (1998).
15. D. D. Edwards and T. O. Mason: Subsolidus phase relations in the Ga_2O_3-In_2O_3-SnO_2 system. *J. Am. Ceramic. Soc.* 81:3285–3292 (1998).
16. L. D. Marks and E. Landree: A minimum entropy algorithm for surface phasing problems. *Acta Crystallogr.* A54:296 (1998).
17. E. Landree, C. Collazo-Davila, and L. D. Marks: Multisolution genetic algorithm approach to surface structure determination using direct methods. *Acta Crystallogr.* B53:916 (1997).
18. M. V. Berry: Diffraction in crystals at high energies. *J. Phys. C* 4:697 (1971).
19. K. Kambe, G. Lehmpfuhl, and F. Fujimoto: Interpretation of electron channeling by the dynamical theory of electron diffraction. *Z. Naturforsch.* 29a: 1034 (1974).
20. F. Fujimoto: Periodicity of crystal structure images in electron microscopy with crystal thickness. *Phys. Stat. Sol.* 45:99 (1978).
21. D. Van Dyck: Image calculations in high-resolution microscopy: Problems, progress and prospects. In *Advances in Electronics and Electron Physics*, vol. 65, P. Hawkes, ed., Academic Press, New York, p. 295 (1985).
22. D. Van Dyck and M. Op de Beeck: A simple intuitive theory for electron diffraction. *Ultramicroscopy* 64:99 (1996).
23. P. B. Hirsch, A. Howie, R. B. Nicholson, D. W. Pashley, and M. J. Whelan: *Electron Microscopy of Thin Crystals*, 2 ed., Robert E. Krieger, Malabar, FL (1977).

24. J. T. Vaughey, J. P. Thiel, E. F. Hasty, D. A. Groenke, C. L. Stern, K. R. Poeppelmeier, B. Dabrowski, D. G. Hinks, and A. W. Mitchell: Synthesis and structure of a new family of cuprate superconductors: $LnSr_2Cu_2GaO_7$. *Chem. Mater.* 3:935 (1991).

25. P. A. Doyle and P. S. Turner: Relativistic Hartree-Fock x-ray and electron scattering factors. *Acta Crystallogr.* 24:390 (1968).

Received February 1998; accepted June 1998.